9-2010

Progressive Failure Simulation of Security Cable Barriers

Christopher Y. Tuan
University of Nebraska-Lincoln, ctuan@unomaha.edu

Ratul D. Sarmah
Schneider Structural Engineering

Alexander Y. Tuan
Tamkang University

Ching-Sheng Kao
Tamkang University

Q. S. Li
City University of Hong Kong

©Freund Publishing House Ltd., International Journal of Nonlinear Sciences & Numerical Simulation 11(9): 753-773, 2010

Progressive Failure Simulation of Security Cable Barriers

Christopher Y. Tuan[1], Ratul D. Sarmah[2], Alexander Y. Tuan[3], Chin-Sheng Kao[4], Q.S. Li[*5]

[1]*Professor, Department of Civil Engineering, University of Nebraska-Lincoln, USA.*
[2]*Senior Engineer, Schneider Structural Engineering, Omaha, Nebraska, USA.*
[3]*Asistant Professor, Department of Civil Engineering, Tamkang University, Taiwan, ROC.*
[4]*Associate Professor, Department of Civil Engineering, Tamkang University, Taiwan, ROC.*
[5]*Associate Professor, Department of Building and Construction, City University of Hong Kong, Kowloon, HK.*
[*] *Corresponding author. Email: bcqsli@cityu.edu.hk (Q.S. Li)*

Abstract

Perimeter security cable barriers are widely used by various agencies all over the world to defeat threat vehicle penetration. New barrier designs require crash test validation prior to implementation. Full-scale vehicular crash tests are costly, whereas designs via finite element simulations are time consuming and require specialized skills. Based on full-scale crash tests, an innovative and simple algorithm has been developed to model the progressive failure of security cable barriers. A multi-body approach based on the first principles of physics was developed to substantially reduce computer runtime. The solution algorithm uses a large number of small time steps. Nonlinear vehicle and cable forces and deformations are calculated based on compatibility conditions. This methodology has been validated against three full-scale crash tests. This cable barrier model, displaying simulation results graphically in a time series, provides realistic response parameters of a security cable barrier design in less than 10 minutes of runtime with reasonable accuracy.

Keywords: vehicular crash, security cable barriers, progressive failure, simulation

Introduction

Perimeter security barriers are routinely used all over the world for stopping vehicle penetration to protect physical facilities. Typical rigid barriers used for perimeter security are reinforced concrete barrier walls and Jersey barrier segments. In other applications, individual or clustered concrete-filled steel pipes (or bollards) have also been used. Flexible barriers are typically cables and container-type barriers. There has always been a need to design for new security barriers, which are functionally efficient, cost effective, constructible using locally available materials and easily installed. In the United States, cable barriers for roadside safety applications are produced by many companies. Recently, cable barriers have attracted much attention from designers developing new perimeter security barriers for low cost and easy installation.

There has been a lot of research on cable barriers, specifically for roadside safety application, which has resulted in a large number of crash tests conducted by transportation agencies. However, in roadside safety application, cable barriers are designed for vehicle's impact angle less than 45 degrees. The primary objectives are to redirect a vehicle to mitigate potential injuries to the passengers

and to contain the vehicle from colliding with oncoming traffic [18]. For security barriers, the impact of the vehicle is commonly assumed to be head-on or 90-degree impact angle, which imposes a larger probability of penetrating the barrier. The primary objective is to arrest the impacting vehicle within a certain range of penetration without concerns about passenger safety.

In recent days numerical simulations using finite element techniques have replaced many costly full-scale crash tests and provided reliable results. However, detailed finite element simulations of crash dynamics are computationally intensive and time-consuming. In this study, an efficient algorithm based on the first principles of physics has been developed for simulation of progressive failure of cable security barriers. The results proved to be reasonably accurate when compared against crash test data, and runtime is typically under 10 minutes on a desktop or a laptop computer. The explicit algorithm using a large number of small time steps (< 0.5 ms) is suitable for analyzing the progressive failure simulation graphically in a time series. These features allow a designer quickly assess the vulnerability of a cable barrier under various vehicular impact scenarios.

Review of simulation algorithms

Since the early 1990s, there has been a large quantity of research on vehicular collisions with roadside hardware as well as inter-vehicular collisions. Two basic approaches have been adopted in the investigations of hardware for roadside safety. In a multi-body simulation approach, individual components are modeled as a series of connected rigid body segments. An example is the two-dimensional algorithm in BARRIER VII [16]. The second approach is the use of many recently developed three-dimensional finite element software programs. NCHRP Report 350 [18] provides an historical perspective and describes a number of the earlier software programs.

Simulation of cable barrier crash dynamics was first published in 2001 [4]. This study investigated a roadside safety wire rope fence and the algorithm developed was based on the analysis of a large amount of roadside safety cable barrier crash test data. The algorithm was validated with crash test data involving small vehicles with acute angle of impact. In 2007, the National Crash Analysis Center (NCAC) of the U.S. Federal Highway Administration at George Washington University conducted performance evaluation of a low-tension, three-strand cable median barrier for roadside safety [13]. A simulation model was developed for a roadside safety cable barrier consisting of three 19-mm cables for small vehicle impact conditions.

Vehicle model

Finite element models of common automobiles have been developed by the National Crash Analysis Center. The models are typically used as input files in the explicit finite element program LS-DYNA [11] for conducting crash dynamics simulation. These models are generally very detailed and contain hundreds of thousands of nodes and elements.

In this study, the finite element model of a 15,000-lb pickup truck developed by NCAC is simplified by substantially reducing the number of nodes and elements while maintaining the same physical configuration. The vehicle is modeled as an assembly of solid elements (i.e., the chassis, engine, gear-box and wheel hubs) surrounded by shell elements (i.e., the sheet metal). The inertial properties of the vehicle are calculated from the mass distribution of the solid elements [19]. The mass densities of individual solid elements can be adjusted for any gross vehicle weight (GVW) of the vehicle. No stiffness properties of these solid and shell elements are considered in the algorithm. Instead, every node of the deformable body (i.e., the shell elements) is connected to a node on the rigid body with a 2-node space truss element. These nodes are selected such that the impact forces developed in the trusses upon collision would yield vehicle trajectories observed in the actual crash tests. Therefore, the selection of the truss

node, number of truss members and the nonlinear stiffness properties of these truss members are based on numerous trials [20] to best fit crash test data.

An algorithm for cable barrier progressive failure analysis

A multi-body explicit algorithm has been developed to simulate the crash dynamics between a vehicle and a cable barrier. The event is divided into small time steps of 0.5 ms or less. During a time step, a three-dimensional vehicle model interacts with a three-dimensional cable barrier model, resulting in deformations in the cables and contact forces. The kinetic and kinematic properties of a vehicle are derived from the physical data provided by the manufacturer [19]. At the start of each time step, the position, the orientation, and the velocities of the vehicle are known from the initial conditions or from the previous time step. The contact forces and the moments at the vehicle center of gravity from impact in the pitch, yaw and roll directions are calculated. The vehicle's accelerations are subsequently computed at the end of each time step from the sum of forces acting on the vehicle CG. Only the failure modes of the cable barriers observed in crash tests are considered in the simulations. Potential failure modes include cable breakage, line/end post failure due to bending and shear, cable anchor pullout, post anchor pullout, and vehicle rolling over the barrier.

Collision Detection

For a security cable barrier, collision generally takes place within a cable bay. As shown in Figure 1, the cables between two adjacent posts anticipating the vehicle collision form a contact surface, which is meshed with a grid of contact nodes. The nodes in the contact surface that collide with a vehicle are moved in the direction of the vehicle. The nodal displacement vector is equal to the distance moved by the vehicle during a time step, less the adjustment made for vehicle crush during that time step. The adjustment in the cable barrier model for vehicle crush is explained later in the paper. For the nodes that are not in contact with the vehicle move along a straight line joining the collision node on either side of the vehicle and the node of the same cable on the nearest post that has not failed. The nodes on a post move with the post until the post fails in base shear or pull out.

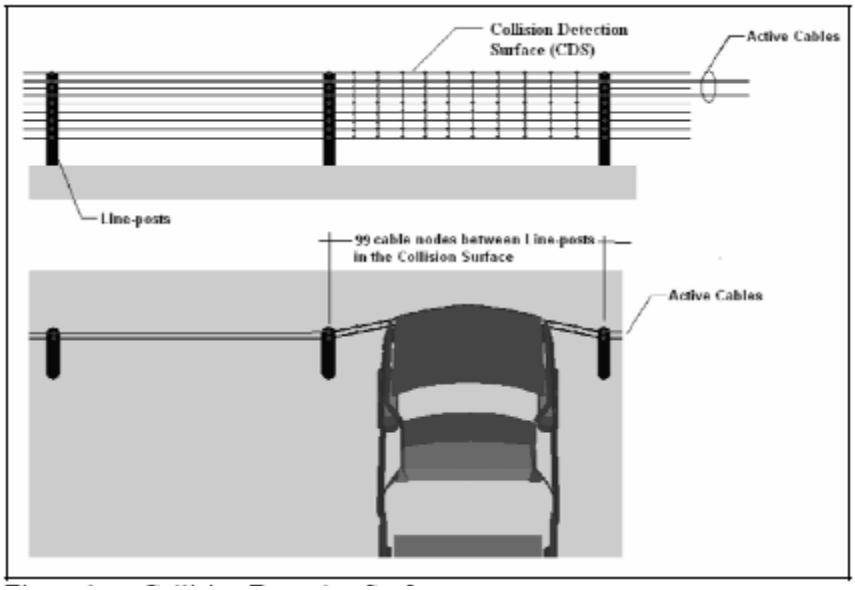

Fig. 1: Collision Detection Surface

Computation of Cable Forces

Upon initial impact, the length of a cable increases as the vehicle penetrates into the cable barrier. The increment in cable tension can be calculated according to the Hooke's law:

$$T_1 - t_1 = \frac{EA\Delta l_1}{l_1} = \frac{EA(L_1 - l_1)}{l_1} \quad (1)$$

$$T_2 - t_2 = \frac{EA\Delta l_2}{l_2} = \frac{EA(L_2 - l_2)}{l_2} \quad (2)$$

where E is the "apparent modulus of elasticity", A is cross-sectional area, T and t are the tensions, and L and l are the effective lengths of the cable. The subscripts 1 and 2 represent the cable bay on the left and right side of the vehicle, respectively, while the lower case and upper case letters represent values before and after an increment of strain, respectively. Change in total length of the cable is denoted by □l .

The Euler model shown in Figure 2 for tension drop over a sheave due to friction may be applied to determine the tension drop on either side of a lodged-in vehicle or over a post between two adjacent cable bays. The two cable tensions are related as follows:

$$T_1 = e^{-\mu\theta} T_2 \quad (3)$$

where $T_1 < T_2$, □ is the coefficient of friction between the cables and the contacting surface of the vehicle or the post, and □is the subtended angle of the contact surface.

The total elongation in a cable is the sum of elongations on the left and right sides:

$$\Delta l = \Delta l_1 + \Delta l_2 \quad (4)$$

Combining Eqs.(1) through (4) yields

$$T_1 = \frac{\Delta lEA + t_1\left(l_1 + e^{-\mu\theta} l_2\right)}{l_1 + e^{-\mu\theta} l_2} \quad (5)$$

and

$$T_2 = \frac{\Delta lEA + t_2\left(l_2 + e^{-\mu\theta} l_1\right)}{l_2 + e^{-\mu\theta} l_1} \quad (6)$$

If there is no friction, the horizontal tension component along a cable will be the same. Since a cable is normally attached to a post or threaded through the posts, this frictional tension drop can be significant.

The cable length between the center of vehicle's front bumper and the anchors on either end of a cable are considered as the effective length. In the event of a post failure due to base shear or pullout, all the cables will instantly become slack and the cable tensions, base shears and pullout forces associated with the failed posts and the anchors are set to zero. At this time instant, the total cable length less the elastic elongation of the cable is stored temporarily and the cable nodes on the failed posts are moved to the adjacent post on the same side of the vehicle. This causes the cable length to shorten and the total cable length to fall below the stored length. As the vehicle moves forward, the cable length will start to increase again. The computation of cable tensions, and post's shear, pullout and anchor pullout forces resumes as soon as the total cable length exceeds the stored value. The resultant cable tension vectors and the resultant moment vectors are applied to the vehicle C.G. in each time step during the simulation. This procedure of progressive failure is continued until either the vehicle is stopped by the cables or the vehicle penetrates the cable barrier, in which case the residual velocity of the vehicle is calculated.

Mechanical Properties of Cables

A cable or a wire rope is formed by individual wires wound into a strand that are

woven together. Initial elongation in a woven cable under an axial tensile force is caused by the stretching of individual strands and the seating of wires against one another. In the wire rope catalog by Wire Rope Industries in Quebec, Canada, a non-galvanized, seven-wire strand has an effective modulus of 62,000 to 69,000 MPa, and galvanized seven-wire strand has an effective modulus of 110,000 MPa (16,000 ksi). Some cable manufacturers have the capability to pre-tension and stretch the cable to partially remove the initial stretches for dynamic loading. This process results in a 25 ~ 30% increase in their effective modulus [1,2]. Table 1 provides properties of commonly used structural wire ropes conforming to ASTM-A603 and galvanized structural strands conforming to ASTM-A584. Even though the nominal strength of galvanized structural strands are higher than that of structural wire ropes, the latter is preferred for cable barrier as its modulus of elasticity is lower, which helps to dissipate kinetic energy more efficiently.

Published data on plastic behavior of cables are not readily available. The yield strength of cable is not clearly defined due to the fact strands being woven together, and stresses under load in each strand is not uniform. At a slow loading rate, stresses in cable will become plastic at about 60% of the nominal tensile strength. ASTM standards hence allow a maximum pre-stretching force at 55% of the nominal strength. Figure 3 shows an idealized stress-strain curve for cables in the simulation. When the cable tension reaches 60% nominal strength during the simulation, Equations (5) and (6) are no longer valid. From this point on in the simulation, the modulus was reduced by 40% and the same equations were used to compute cable tension until cable strength reached nominal strength. Beyond the nominal strength, a cable is assumed to deform plastically. Using the stress-strain curve of a pre-stressing strand given in the PCI Design Handbook, strain at this point was assumed at 0.015% and a constant cable tension was maintained until a maximum strain of 0.03%, which is the breaking point of the cable.

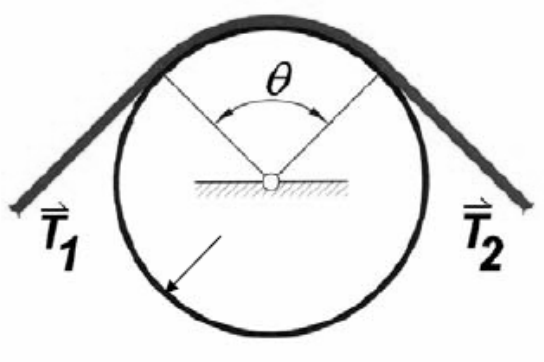

Fig. 2: Tension Drop over a Sheave

Post modeling

Post behavior under dynamic loading depends upon various parameters such as post material, inertial properties and type of cable attachment, foundation embedment depth and soil properties. Post behavior under vehicular impact has been studied extensively [5,9,10,12], generally based on crash simulations and validation with crash test results. Interaction of post with soil has been discussed in [6,8,12,15,17,21]. Forces exerted on a post by the cables are resisted by a shear force and a moment at the base of the post. From these studies, elasto-plastic response of post failure under dynamic lateral load can be assumed to remain elastic up to a maximum moment capacity, Mp, at which a plastic hinge develops at the base of the post.

Dynamic Testing on Posts in Soil

Dynamic testing of W6×16 steel posts in soils was conducted [12,17] using a 2,237-lb rigid-frame body vehicle (i.e., a bogie) to evaluate the effects of embedment depths as well as to determine the associated force deflection characteristics. The steel posts were embedded in soils conforming to AASHTO M147-65 Gradation B specification. The steel guardrail posts were impacted at a target speed of 20 mph. An impact head, fabricated from an 8-inch diameter concrete-filled steel pipe and used to strike the posts, was mounted to the front end of the bogie vehicle at a height 24.875 in. above the ground.

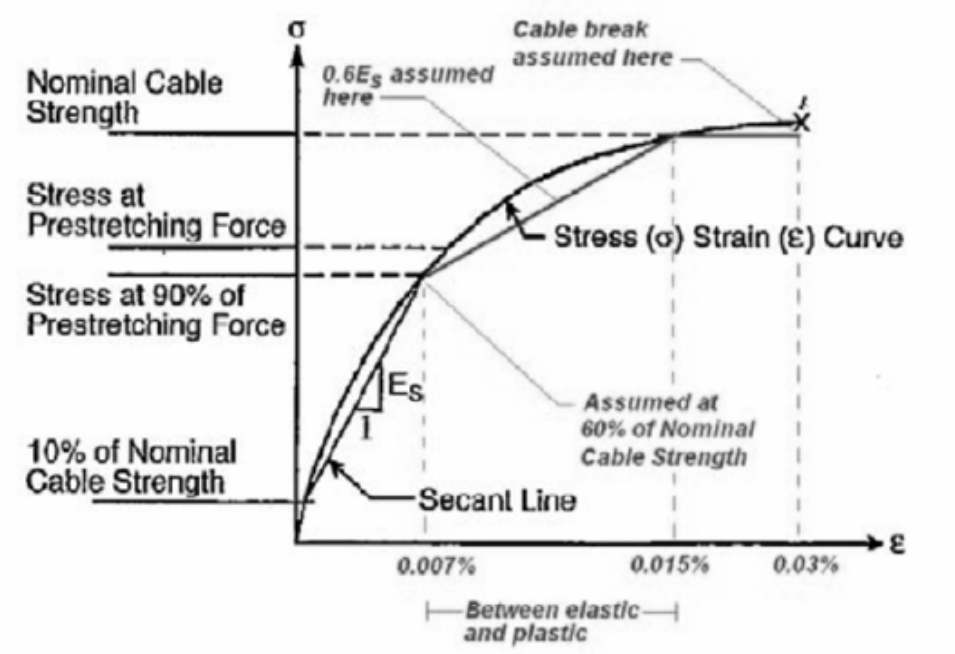

Fig. 3: Idealized Stress-strain Curve of Cable used in Simulation

A total of ten impact tests [12] were performed on the embedded steel posts. Actual impact conditions, post embedment depths and test results are given in Table 2. All steel posts were impacted to cause bending about the post's strong axis. Failures of the posts were found to be dependent upon the embedment depth. For post embedment depths of 1,016 mm or greater, soil failure was evident with slight yielding within the post. For post embedment depths of 940 mm or less, the posts were pulled out of the ground after rotating in the soil for some distance. In addition, there were measurable differences in the impact forces observed for the two modes of failure. As a result of these differing impact forces, the amount of energy dissipated also varies. Post that failed by rotating in the soil dissipated more energy than posts than the posts that initially rotated but eventually pulled out of the ground.

Algorithm for Post Behavior Simulation

Typical post deformation is illustrated in Figure 4. For post immediately adjacent to vehicle, node B is on the contact surface and corresponds to the colliding cable node at the extreme end of vehicle bumper or body. For any other cable bay, the node B corresponds to a node on the same cable on the adjacent line post towards the vehicle. Similarly, in the end cable bay, the node A represents the cable node on the anchor, and for any other cable bay, the node A corresponds to a node on the same cable on the adjacent line post towards the anchor. The node O represents the cable node on the current post where it is attached to the post. The vector B represents the resultant tensile force on the current post by the cables during the time step. C represents the node rigidly attached to the post base.

The tension along OB is computed by

$$\vec{T}_{OB} = \vec{R} \cdot \left(\hat{OB} \right) \tag{7}$$

where R (T1 or T2) is computed from Equation (5) or (6). The horizontal component of T1 or T2 at adjacent posts gradually decreases from vehicle to the anchor on either side of the

vehicle. This drop in cable tension is computed by using Equation (3). Therefore, vectors TOB and TOA can be computed at all posts for all cables. Further, the resultant cable tension is

$$\vec{R} = \vec{T}_{OA} + \vec{T}_{OB} \tag{8}$$

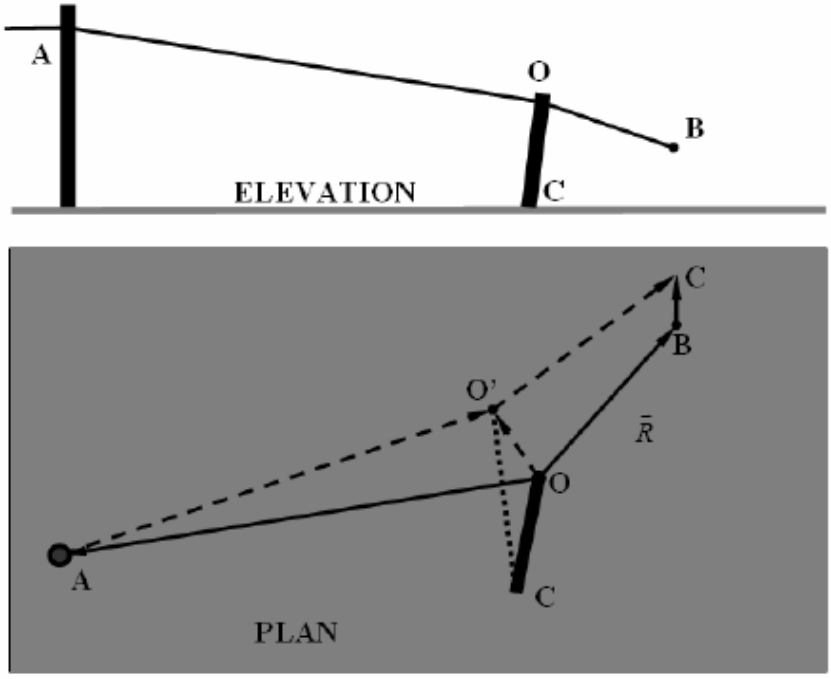

Fig. 4: Deformation of Line-post/pull-post

Table 1
Wire rope product information

STRUCTUTAL WIRE ROPES - Conforming to ASTM A603-98 - Standard Specification for Zinc-Coated Steel Structural Wire Rope					
Rope Diameter		Approx. Weight	Metallic Area	Nominal Strength (Class A Coating)	Apparent Modulus of Elasticity
inch	mm	lb/ft	in2	kips	ksi
1/2	13.0	0.42	0.119	23.0	20,000
3/4	19.0	0.95	0.268	52.0	20,000
1	26.0	1.67	0.471	91.4	20,000
SPIRAL STRAND - Conforming to ASTM A586-3 - Galvanized Structural Strand					
Rope Diameter		Approx. Weight		Nominal Strength (Class A Coating)	Apparent Modulus of Elasticity
inch	mm	lb/ft		kips	ksi
1/2	13.0	0.52		30.0	24,000
3/4	19.0	1.18		68.0	24,000
1	26.0	2.1		122.0	24,000

Table 2
Steel Post Impact Test Results

Test No.	Impact Speed (mph)	Embedment Depth (mm)	Total Deflection (mm)	Total Energy (ft-lb)	Failure Mode
NPGB-1	20.00	1092	1045.3	21,994	Post rotation, slight yielding
NPGB-2	21.00	1016	1152.9	21,500	Post rotation
NPGB-3	20.00	1092	1241.7	20,984	Post rotation, slight yielding
NPGB-4	20.00	1016	1092.3	21,493	Post rotation
NPGB-5	20.00	940	1365	20,187	Post pulledout of ground
NPGB-6	20.49	864	1340.1	17,849	Post pulledout of ground
NPGB-7	19.71	940	1326.3	16,595	Post pulledout of ground
NPGB-8	20.69	940	1164.1	18,314	Post pulledout of ground
NPGB-9	20.76	1016	1221.5	21,507	Post rotation, slight yielding
NPGB-10	21.50	1016	1185.6	23,440	Post rotation, slight yielding

and the resultant moment vector about the base C is,

$$\vec{M} = \vec{OC} \times \vec{R} \quad (9)$$

The deflection at the post top shown in Figure 5, y1 + y2, is given by Equation (11), in which R is the perpendicular to post component of R,

$$\theta_P = \frac{RL_1^{\,2}}{2EI} \quad (10)$$

$$y_1 + y_2 = \frac{RL_1^{\,3}}{3EI} + L_2(\tan\theta_P) \quad (11)$$

With the displacement vector, (y1 + y2), the rotation angle □ between the original and new positions of the post (OC and OC') can be determined. Finally, with the rotation angle vector, α, the new position vector for the post can be determined as follows:

$$\vec{V} = \vec{V} \times \left\{ \vec{I} + \left[\frac{\sin(d)}{d} \vec{L} \right] + \left[\left(1 - \frac{\cos(d)}{d^2} \right) \vec{L} \times \vec{L} \right] \right\} \quad (12)$$

where $V = [v_x, v_y, v_z]$ is the rotation vector, I = 3x3 identity matrix, $\vec{\alpha} = [\alpha_x, \alpha_y, \alpha_z]$ is the rotation angle vector,

$$L = \begin{bmatrix} 0 & l_z & -l_y \\ -l_z & 0 & l_x \\ l_y & -l_x & 0 \end{bmatrix}$$

is the rotational matrix formed from elements of rotation angle vector, and $d = \sqrt{l_x^2 + l_y^2 + l_z^2}$.

Equations (7) through (12) are valid as long as the post base moment, $|\vec{M}| < M_p$, where $M_p = Z_x F_y$, denotes the plastic moment of the post, Z_x the plastic modulus of the post, and F_y the yield stress of the post.

When the base moment, $|\vec{M}| \geq M_p$, the

following steps are used to compute post deflection. As illustrated in Figure 6, the direction of movement of node O, n, can be computed as

$$\vec{n} = \left[\vec{OC} \times \left(\vec{OA} + \vec{OB} \right) \right] \times \vec{OC} \tag{13}$$

and the displacement from O to O' is denoted as in the direction of n. The new displacement vectors, O′B and O′A, can be expressed as

$$\vec{O'B} = \vec{OB} - \delta(\hat{n}) \tag{14}$$

$$\vec{O'A} = \vec{OA} - \delta(\hat{n}) \tag{15}$$

The decreases in the cable lengths due to changes in cable tensions are computed as

$$\Delta_1 = |\vec{OA}| - |\vec{O'A}| = \frac{\Delta T_1 \, |\vec{OA}|}{AE} \tag{16}$$

$$\Delta_2 = |\vec{OB}| - |\vec{O'B}| = \frac{\Delta T_2 \, |\vec{OB}|}{AE} \tag{17}$$

where ΔT_1 and ΔT_2 are changes in the cable tensions.

The new cable force vectors along O′B and O′A are computed as follows,

$$\vec{T}_1' = \left(T_1 - \Delta T_1 \right) \hat{O'A} \tag{18}$$

$$\vec{T}_2' = \left(T_2 - \Delta T_2 \right) \hat{O'B} \tag{19}$$

The base moment, M′, is updated by iterating till the following condition is satisfied.

$$|\vec{M}'| = |\vec{O'C} \times \left(\vec{T}_1' + \vec{T}_2' \right)| \le M_p \tag{20}$$

The final deflection vector at the top of the post is updated as $\delta(\hat{n})$.

This procedure of computing the post deflection is carried out until a maximum post rotation has reached, at which a post can no longer take additional moment. In this study, a maximum rotation angle between the final post orientation and the ground is set at 45 degrees.

Adjustment for vehicle deformation

Computation of the contact forces in the simulation of vehicle-barrier crash dynamics must satisfy consistent deformations. At the end of each time step, the colliding nodes of the vehicle after deformation must lie on the contact faces of the barrier and vice versa. No separation or overlapping between the vehicle and barrier contact faces is allowed for the solution to converge. The deformations of the vehicle and the barrier depend upon their respective stiffness values. Thus the computation of the deformations and contact forces in traditional finite element simulations is iterative and computationally intensive.

Since a cable barrier is relatively more deformable than a vehicle, and deformation in the vehicle is initially ignored to expedite the solution runtime. To correct this error, crash test data from the vehicle impacting a rigid barrier is used. Since there is little energy absorbed by a rigid barrier, the crash test provides vehicle deformation information with respect to energy absorbed by the vehicle and impact forces transferred to the vehicle. The relationship between vehicle deformation and the impact force is incorporated directly in the algorithm without actually modeling the vehicle deformation. Figure 7 shows the relation between the “average” deformation of a 15,000-lb pickup truck with a rigid barrier at 39.25-mph impact speed and 91.5-degree impact angle. If crash test data is not available,

numerical simulation data using a validated vehicle model may be used instead.

The following steps are used to include the effect due to vehicle deformation: (1) the average vehicle deformation and normal impact force data are stored for the vehicle model in a simulation; (2) during each time step of the simulation, the vehicle deformation is determined based on the impact force exerted by the cable on the vehicle; (3) the cable deformation in the same time step is reduced by the computed vehicle deformation. Cable tensions are recalculated based on the adjusted cable deformation; and (4) repeat steps (2) and (3) until the change in cable tensions is less than a tolerance (e.g., < 5%). This algorithm expedites the runtime significantly without compromising the simulation accuracy.

Validation of the algorithm against crash tests

Three crash tests, APS1, APS3 and APS4, conducted by the Texas Transportation Institute on perimeter security cable barriers are used to validate the algorithm developed herein. The criteria specified by the Department of State, SD-STD-02.01, for the performance level K8/L2 were followed in these crash tests.

Crash Test #APS1

The cable barrier was constructed with cold-formed 4-in. deep I-beam posts, spaced at 8 ft on centers, supporting open trapezoidal horizontal rails with a 2.5 in. by 2 in. cross-section. Four horizontal rails were located at 1 ft, 2.5 ft, 4 ft and 7 ft above grade, respectively. The total length of the cable barrier was 152 ft. Hollow structural shapes (HSS) 4 in.×4 in.×1/8 in. were used for anchor posts placed at either end of the barrier and spaced 48 ft apart. All anchor posts were filled with 3,000-psi concrete. Intermediate anchor posts were installed in 8 ft by 3 ft by 4 ft. deep concrete footing. Each dead-man anchor was 8 ft by 6 ft by 4 ft deep concrete footing. All line posts were installed in 18-in. diameter by 3 ft deep footings. Cables of 1.5-in. diameter were threaded continuously through holes in the rails located at 2.5 ft and 4 ft above grade. The crash test layout and impact scenario of the cable barrier are shown in Figure 8. The time-histories of vehicle deceleration from the crash test are compared with those from the simulation in Figure 9. Figure 10 compares the snapshots taken from high speed crash test video and from the simulation run at different times.

Crash Test #APS3

The cable barrier was constructed with cold-formed 1.75 in.× 4 in. I-beam posts, spaced at 8-ft on centers, supporting open trapezoidal horizontal rails with a 2.5 in. by 2 in. cross-section. Four horizontal rails were located at 1 ft, 2.83 ft, 4 ft and 7 ft above grade, respectively. The total length of the cable barrier was 136 ft. Unreinforced concrete, 3-ft diameter by 5-ft deep, footings were used as dead-man anchors installed at both ends. Two intermediate footings, 3-ft diameter by 5-ft deep, were installed 56 ft from the dead-man anchors. Line posts were installed in 9-in. diameter by 3-ft deep concrete footings. The concrete was specified to be 6,000 psi. Cables of 1.75-in. diameter were threaded continuously through holes in the rails located at 2.83 ft and 4 ft above grade. All cables were attached to the anchor foundations by 1.25-in. diameter cable clamps embedded with helical anchors. The crash test layout and impact scenario of the cable barrier are shown in Figure 11. The time-histories of vehicle deceleration from the crash test are compared with those from the simulation in Figure 12. Figure 13 compares the snapshots taken from high speed crash test video and from the simulation run at different times.

Crash Test #APS4

The cable barrier was constructed with cold-formed 1.75 in.× 4 in. I-beam posts, spaced at 8.17-ft on centers, supporting open trapezoidal horizontal rails with a 2.5 in. by 2 in. cross-section. Four horizontal rails were located at 1 ft, 2.83 ft, 4 ft and 7 ft above grade, respectively. The total length of the cable

barrier was 162.33-ft. Anchor posts made of HSS 4 in.×4 in.×1/8 in. were placed along the barrier and spaced at 32.67-ft on centers. All anchor posts were installed in 3-ft diameter by 6-ft deep footing backfilled with concrete. Line posts were installed in 9-in. diameter by 3-ft deep concrete footings. The concrete were specified to be 6000 psi. Cables of 1.1-in. diameter were threaded continuously through holes in the rails located at 2.83 ft and 4 ft above grade. The crash test layout and impact scenario of the cable barrier are shown in Figure 14. The time-histories of vehicle deceleration from the crash test are compared with those from the simulation in Figure 15. Figure 16 compares the snapshots taken from high speed crash test video and from the simulation run at different times.

Discussions on the Simulation Results

The simulation results of the three crash tests are presented along with the test data in Table 3. The results compare favorably with the crash test data, given the complexity of the dynamic problem. The snapshot comparisons presented in Figures 10, 13 and 16 further demonstrate that the simple algorithm is an efficient simulation tool. This simple cable barrier model provides realistic values for a complex design problem in very reasonable runtime of less than 10 minutes.

The deviation of simulation results from crash test data may be partly attributable to the analysis used to predict the ultimate strengths of the structural components and hardware in a cable barrier. For instance, the post shear failure is assumed to take place only at the interface between the foundation and post.

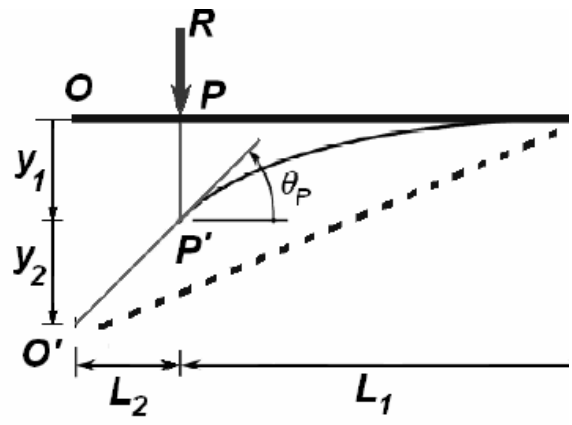

Fig. 5: Deflection of a Cantilever Beam due to a Point Load

The ultimate post shear strength is calculated as 0.6AwFy per American Institute of Steel Construction Design Manual. However, the ultimate shear strength of materials under high strain rate impact loading may well exceed this static value. Another source of error is that the horizontal rails and vertical bars were not included in the cable barrier models. These steel members sustained significant deformation during impact. Some of the vehicle's kinetic energy would have been converted into kinetic energy and strain energy of these members.

Table 3
Comparison of Simulation Results with Crash Test Data

APS1	Crash Test	Simulation
Max 50-ms average Deceleration	-1.485 g	-1.247 g
Exit Vehicle Speed	31.2 mph	29.4 mph
Time elapsed when cable 1 broke	0.088 sec	0.255 sec
Time elapsed when cable 2 broke	0.123 sec	0.295 sec

Table 3 Cont'd:

APS3	Crash Test	Simulation
Max 50-ms average Deceleration	-3.9 g	-2.17 g
Maximum Barrier Deflection	7.49 m	6.78 m
Exit Vehicle Speed	stopped	stopped
Time elapsed until Vehicle Stopped	0.950 sec	0.998 sec
Post Failed in shear/pullout	4 posts on each side of vehicle	4 posts on each side of vehicle

APS4	Crash Test	Simulation
Max 50-ms average Deceleration	-5.72 g	-4.98 g
Maximum Barrier Deflection	4.4 m	6.6 m
Exit Vehicle Speed	stopped	stopped
Time elapsed until Vehicle Stopped	0.78 sec.	0.720 sec.
Post Failed in shear/pullout	4 posts on each side of vehicle	4 posts on each side of vehicle

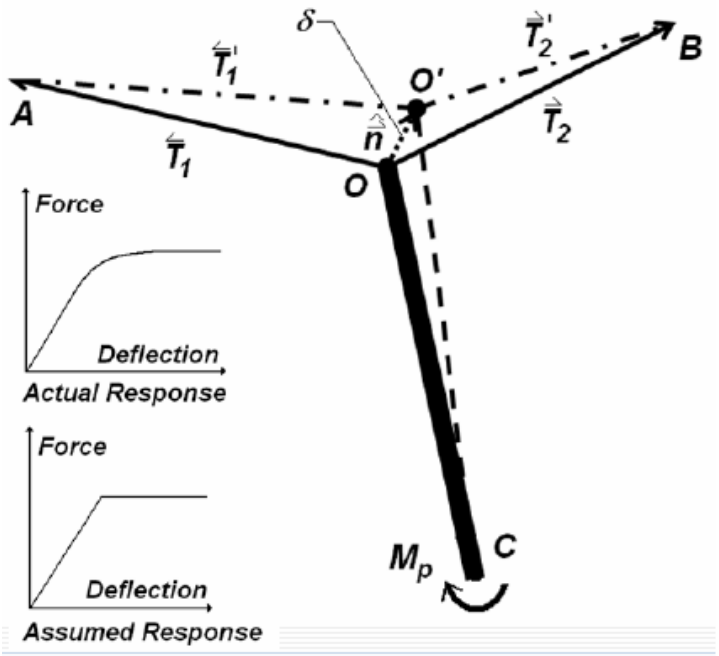

Fig. 6: Post rotation at base under Mp

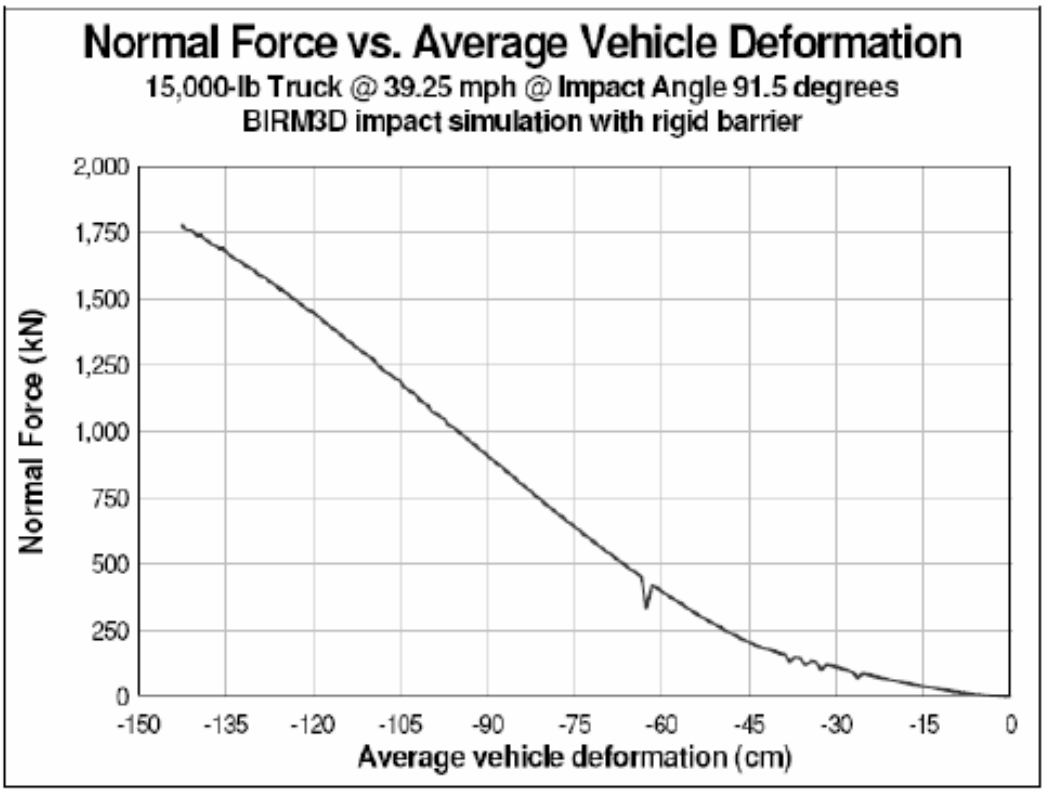

Fig. 7: Normal force vs. Average vehicle deformation in impact with a rigid barrier

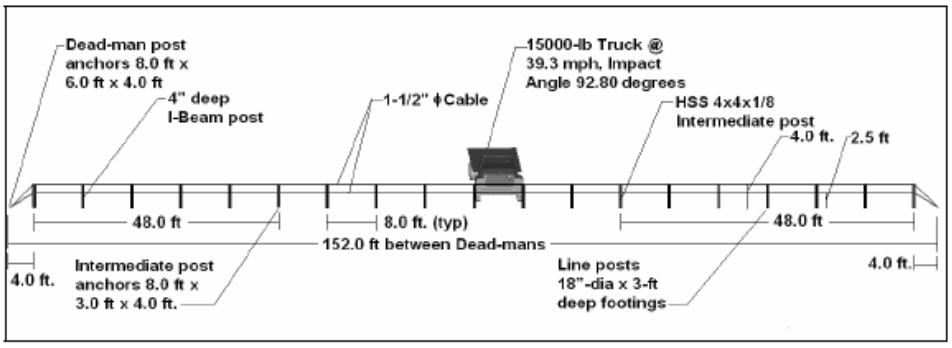

Fig. 8: CRASH TEST # APS1 Impact Scenario

The design of a cable barrier typically requires foundation or anchorage that can sustain large pullout forces, such that the cables can sustain large deformation to dissipate the vehicle's kinetic energy. Thus it usually takes relatively long duration for a cable barrier to bring a vehicle to rest.

Kinetic energy dissipation due to post pullout

There are many publications on post-soil interaction with impact scenarios similar to the current study. In 1970, Southwest Research Institute conducted tests of post-soil interaction

[14]. The test matrix included two soil types, three different posts and four embedment depths. The shear strength of soil was found related to the energy dissipation, and the embedment depth proved to be an important factor. In 1978, Southwest Research Institute conducted pendulum tests [10] on two guardrail posts in five different types of soils. The study focused on properties of posts but did not consider soil characteristics. In a later study, a series of static and dynamic tests was conducted using steel and wooden posts [21] in cohesive and non-cohesive soils. This study predicted that stresses resisting the movement of the post are acting on the leading and trailing faces of the post. In 1996, soil behavior during impact on posts was closely studied [17], where soil pressure along the posts was measured. Test results showed that the shear strength and the modulus of soil had dramatic effects on the responses of the timber and the steel posts tested. The differences in the failure mechanism between stiff and soft cohesive as well as stiff and soft non-cohesive soils were demonstrated by both stress distributions measured by the pressure transducers along the post embedment depths. It is a common design practice of post foundation to assume the point of rotation of a post under lateral loading to be at a depth 2/3 of the post embedment depth from the top of the foundation. This assumption is proved fairly accurate from the plots of soil pressure at different depth during the impact for different soils [17]. In a study in 2005 [3], an optimum depth for a guardrail post was evaluated using LS-DYNA to prevent the impacting vehicle's wheel from snagging with the post. In another study [21], interaction between a guardrail post and gravel was modeled in LS-DYNA and the simulation was validated against crash test.

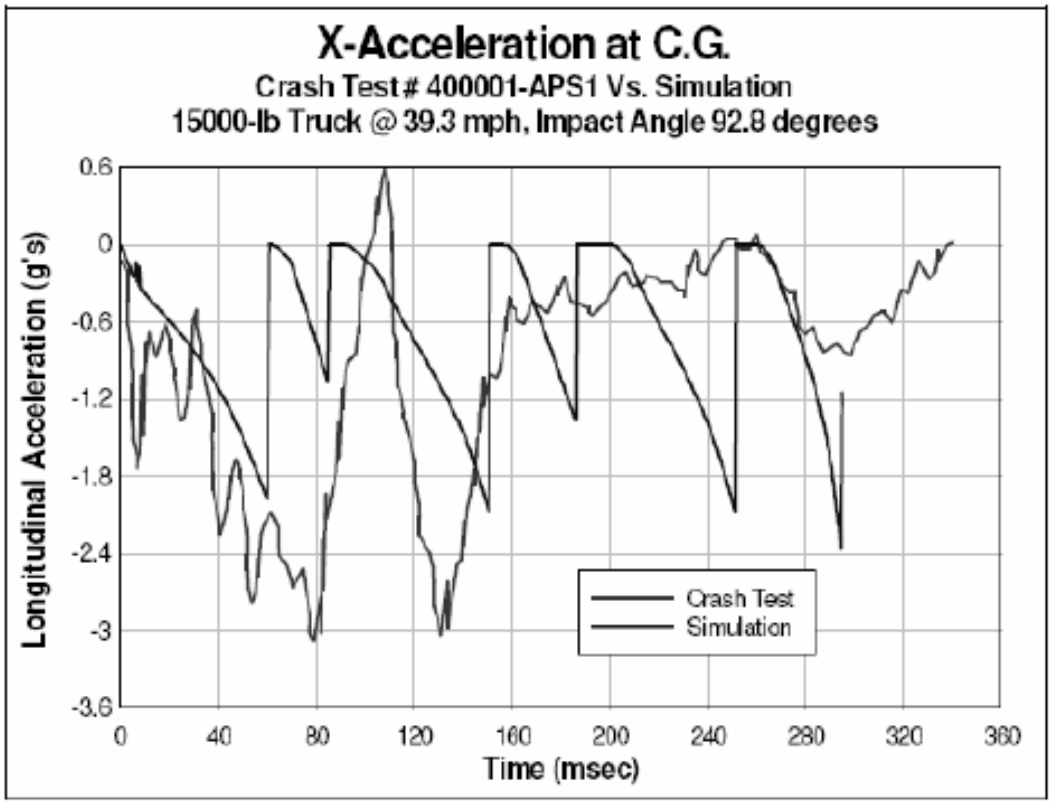

Fig. 9: Comparison of Decelerations at C.G.
Crash Test APS1 vs. Simulation

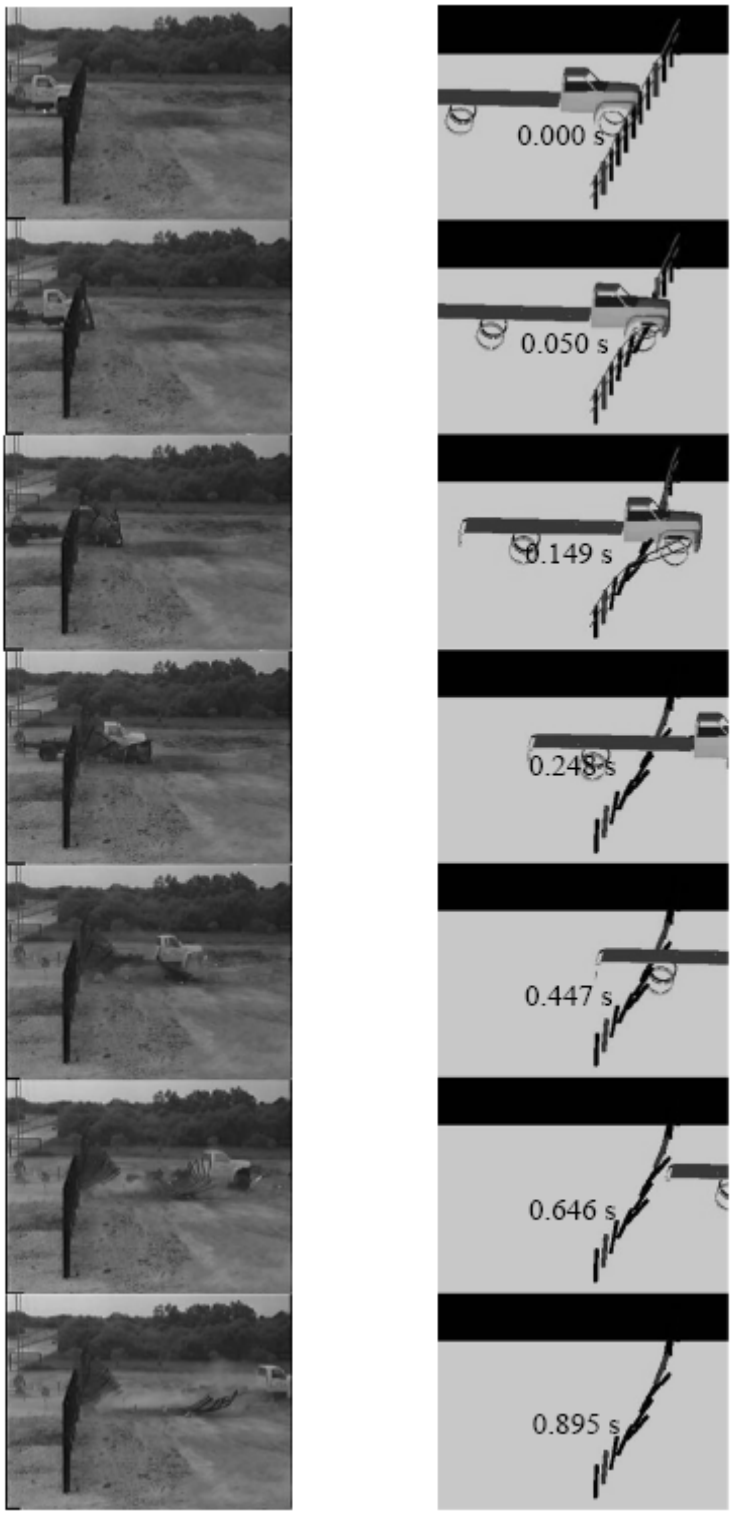

Fig. 10: Snapshot Comparison between Crash Test #APS1 vs. Simulation

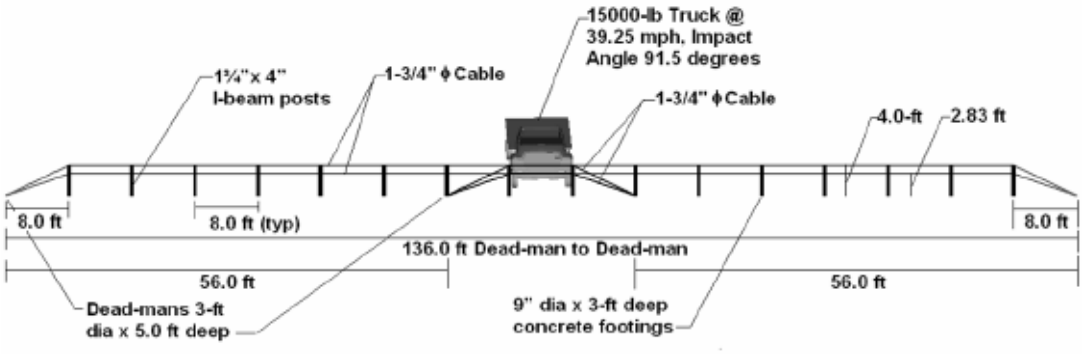

Fig. 11: CRASH TEST #APS3 Impact Scenario

Since the effect of post-soil interaction is critical, it was taken into account in the simulation algorithm. The amount of total energy that can be dissipated in soil-post interaction was empirically estimated based on standard post foundation design. For a concrete foundation in non-cohesive soils with 6~7% moisture content and standard compaction, the post dynamic displacement and kinetic energy dissipated during impact can be related as follows:

$$S_1BD^2 - 2.37PD - 2.64PH = 0 \quad (21)$$

where P is the horizontal load in lbs, H is height above ground for horizontal thrust in feet, B is the average diameter of embedded portion of pole in feet, and S1 is average soil pressure above the point of rotation in psf, and D is the depth of embedment in feet. The maximum value of S1 is set at 8000 psf as the soil bearing strength under dynamic loads. Table 4 shows estimates of the total energy dissipated in the crash tests based on the Equation (21). The kinetic energy of the vehicle was reduced by this value to balance the energy at the end of each time step in the simulation. After taking the energy dissipation into account, simulation results match closely with the crash test results. No energy lost was assumed for crash test #APS1. Further, depending upon the types of anchor, an ultimate pullout capacity of 20 to 50 kips along the post was assumed in the simulation.

Conclusions

The following conclusions are drawn from the current study:

The algorithm developed for simulation of progressive failure of cable barriers is a substantial departure from the conventional finite element techniques. First principles of physics are applied directly to predict the kinetic and kinematic parameters within 10~15% difference from crash test data. Simulations are accomplished in less than 10 minutes of runtime on a desktop or a laptop computer.

The model developed could be further improved by including the post-soil interaction in the simulation, and by accurately modeling plastic stretching of cables as more test data become available.

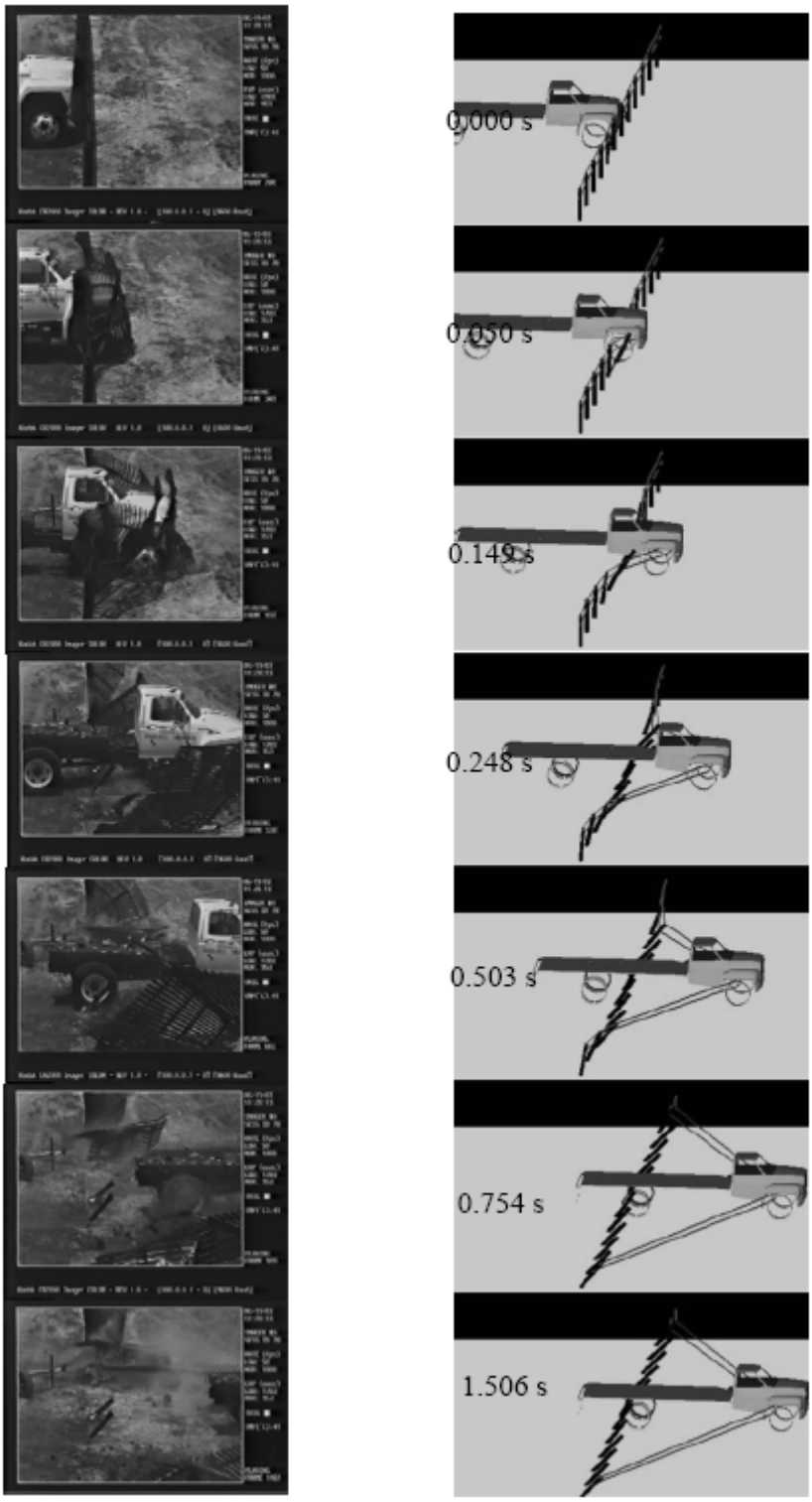

Fig. 12: Comparison of Decelerations at C.G.
Crash Test APS3 vs. Simulation

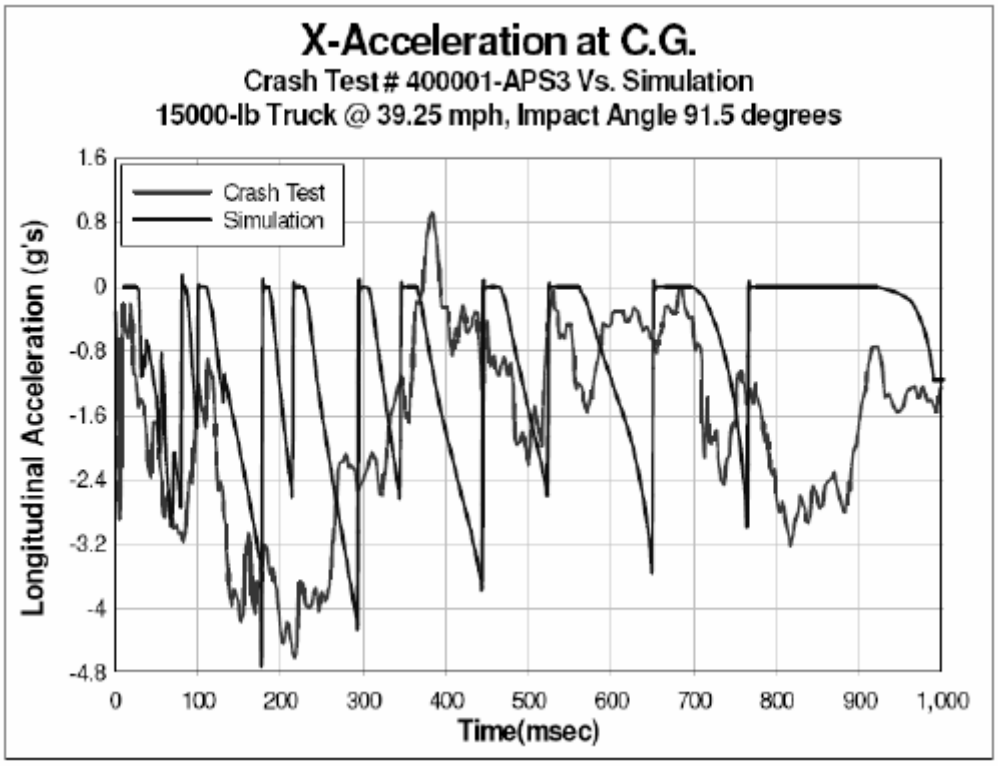

Fig. 13: Snapshot Comparison between Crash Test #APS3 vs. Simulation

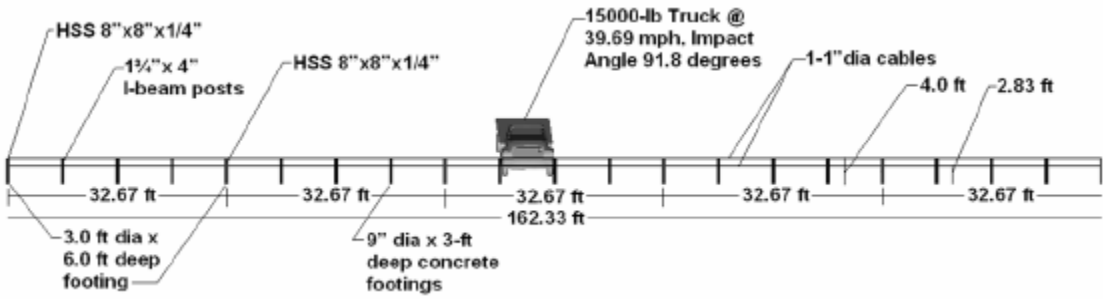

Fig. 14: CRASH TEST #APS4 Impact Scenario

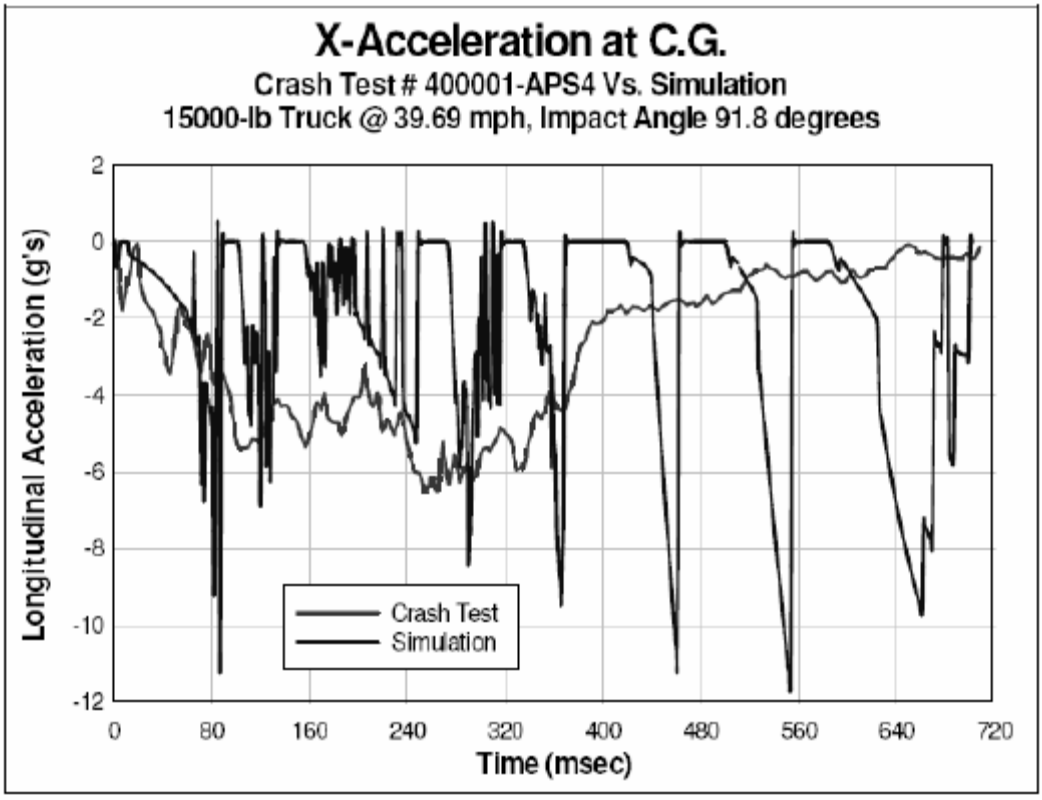

Fig. 15: Comparison of Decelerations at C.G.
Crash Test APS4 vs. Simulation

Table 4
Estimation of Energy Dissipation in Post-Soil Interaction

Literatures on simulations validated with crash test
2000-kg vehicle with 102.2 km/hr @ 25.40 impact angle
K.E. normal to post ~ 270,000 lb-ft. [7]

B	D	δ	Energy absorbed
ft	ft	ft	ft-lbs.
0.479	3.668	0.482	2408
0.479	3.504	0.689	3474
0.479	3.340	0.965	4693
0.479	3.176	1.381	6237
0.479	3.012	1.795	4801

Seen & Estimated from crash test videos

					APS3			APS4		
					# of	Assumed	Energy	# of	Assumed	Energy
S_1	B	D	H	P	post	δ	absorbed	post	δ	absorbed
psf	ft	ft	ft	lb		ft	ft-lbs.		ft	ft-lbs.
8000	0.750	3.000	3.000	3593	2	2	14371	4	2	28743
8000	0.750	3.000	3.000	3593	7	1	25150	13	1.5	70060
8000	1.500	3.000	3.000	7186						
8000	3.000	5.000	3.000	30349	4	1.5	182094			
8000	3.000	6.000	3.000	39024				4	1.5	234146
8000	8.000	4.000	3.000	58851						
8000	8.000	4.000	3.000	58851						
TOTAL					13		221615	21		332949

Standard Pole Foundation Equations where point of zero stress is at a distance of 2/3rd of post depth below ground level

$$S_1 BD^2 - 2.37PD - 2.64PH = 0$$

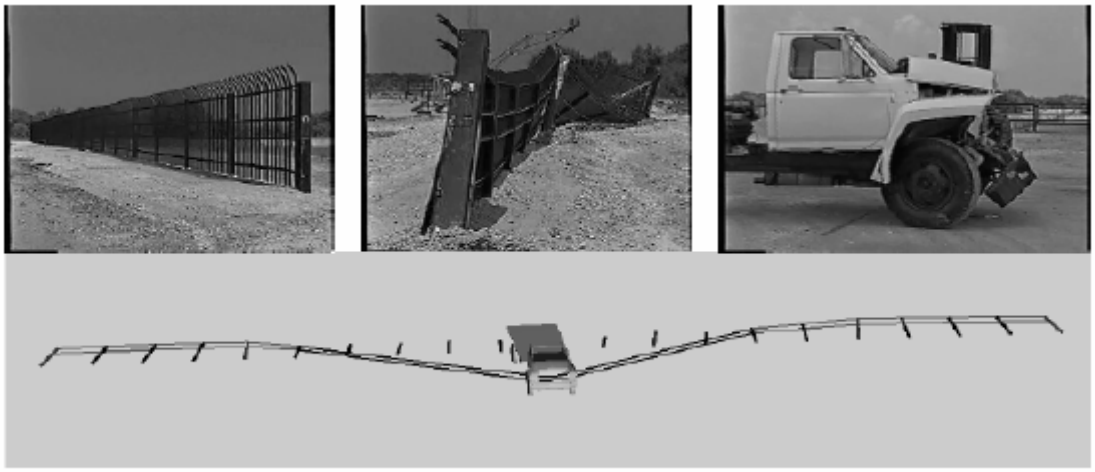

Fig. 16: Comparison of Damage to test vehicle and barrier, Crash Test vs. Simulation

The algorithm developed can be easily adapted to model other passive security barriers, such as concertainers and portable plastic barriers filled with water or sand.

In designing perimeter security cable barrier for K12 impact condition, L1 performance level can be easily achieved. While perimeter security cable barrier can be designed for K12/L2 performance level, it is difficult to achieve L3 performance level, mainly due to the flexible nature of a cable barrier.

Post-soil interactions significantly affect the performance of security cable barrier. Proper selection of posts, cables, post spacing, post and cable anchor foundation sizes and embedment depth are necessary to maximize the kinetic energy dissipation to optimize the barrier performance.

References

[1] Alberson, D.C., R.P. Bligh, C.E. Buth, and D.L. Bullard, Cable and wire rope barrier design consideration, Transportation Research Record No. 1851, 2003, pp. 95-104.

[2] Alberson, D. C., Report on NCHRP Project 20-7(210), Cable barrier – Research and district experiences, update on guidelines for the selection of cable barrier systems, Texas Transportation Institute, , October 11, 2006.

[3] Atahan, A.O., Cansiz, O.F., Improvements to G4(RW) strong-post round-wood, w-beam guardrail system, Journal of Transportation Engineering, volume 131, issue 1, January 2005.

[4] Bateman, M. B., I.C. Howard, A.R. Johnson, and J.M. Walton, Computer simulation of the impact performance of a wire rope safety fence, International Journal of Impact Engineering 25, 2001, pp. 67-85.

[5] Benson, D.J. and Hallquist, J.O., The application of DYNA3D in large scale crashworthiness calculations, Lawrence Livermore National Laboratory, Report No. UCRL-94028, 1986.

[6] Calcote, R. and Kimball, C.E., Properties of guardrail posts for various soil types, Transportation Research Record 679, TRB, National Research Council, Washington D.C., 1978 pp 22-25.

[7] Chaplin, C.R., Failure mechanism in wire ropes, Engineering Failure Analysis, vol-2, issue-1, pp 45-57, March 1995.

[8] Dewey, J.F., Jeyapalan, J.K., Hirsch, T.J., and Ross, H.E., A study of the

soil-structure interaction behavior of highway guardrail posts, Research Report 434-1, Texas Transportation Institute, Texas A&M University, College Station, July1983.

[9] Faller, R.K., Polivka, K.A., Kuipers, B.D., Bielenberg, R.W., Reid, J.R., Rohde, J.R. and Sicking, D.L., Midwest guardrail system for standard and special applications, Transportation Research Record No.1890, pp 19-33, December 2004.

[10] Gentry, T. R. and Bank, L. C., Finite-element modeling and model verification of steel w-beam guardrails subject to pendulum impact loading, Transportation Research Record No. 1647, pp 147-157, November 1998.

[11] Hallquist, J.O., LS-DYNA User's Manual, Livermore Software Technology Corporation, Livermore, California.

[12] Kuipers, B.D. and Reid, J.D., Testing of W152x23.8 (W6x16) steel posts – soil embedment depth study of the midwest guardrail system, MwRSF Research Report No. TRP-03-136-03, Final Report to the Midwest State' Regional Polled

[13] Fund Program, Midwest Roadside Safety Facility, University of Nebraska-Lincoln, Nebraska, June 12, 2003.

[14] Marzougui, D., Mohan, P., Kan, C.D., and Opiela, K, Performance evaluation of low-tension three-strand cable median barriers, Transportation Research Record: Journal of the Transportation Research Board, No.2025, Washington D.C., 2007, pp 34-44.

[15] Michie, J.D., Response of guardrail posts during impact, Research Report 03-9051, Southwest Research Institute, San Antonio, TX, October, 1970.

[16] Plaxico, C. A., Patzner, G. S and Ray, M. H., Finite-element modeling of guardrail timber posts and the post-soil interaction, Transportation Research Record No. 1647, pp 139-146, November 1998.

[17] Powell, G.H., BARRIER VII: A Computer program for evaluation of automobile barrier systems, prepared for Federal Highway Administration, Report No. FHWA RD 73-51, April 1973.

[18] Rohde, J.R., Rosson, B.T., Smith, R., Instrumentation for determination of guardrail-soil interaction, Journal of the Transportation Research Board, National Research Council, Washington, D.C., pp. 109-115, 1996.

[19] Ross, H.E., Jr., Sicking, D.L., Zimmer, R.A., and Michie, J.D., NCHRP Report 350: Recommended procedures for the safety performance evaluation of highway features, TRB, National Research Council, Washaington, D.C., 1993.

[20] Sarmah, R.D., C.Y. Tuan, and E.T. Foster, Three-dimensional barrier impact response modeling (BIRM3D), Proceedings of the 2nd International Conference on Structural Engineering, Mechanics and Computation, Cape Town, South Africa, 5-7 July 2004.

[21] Sarmah, R.D., "Simulations of Progressive Failure of Cable Barriers," a Ph.D. Dissertation, Department of Civil Engineering, University of Nebraska-Lincoln, Lincoln, Nebraska, U.S.A., May 1998.

[22] Wu, W. and Thomson, R., A study of the interaction between a guardrail post and soil during quasi-static and dynamic loading, International Journal of Impact Engineering, 2006.